Multiple-Path Dissociation Mechanism for Mono- and Dinuclear Tris(hydroxamato)iron(III) Complexes with Dihydroxamic Acid Ligands in Aqueous Solution

Hakim Boukhalfa and Alvin L. Crumbliss*

Department of Chemistry, Duke University, Box 90346, Durham, North Carolina 27708-0346

Received February 15, 2000

Linear synthetic dihydroxamic acids ($[CH_3N(OH)C{=}O)]_2(CH_2)_n$; H_2L^n) with short ($n = 2$) and long ($n = 8$) hydrocarbon-connecting chains form mono- and dinuclear complexes with Fe(III) in aqueous solution. At conditions where the formation of $Fe_2(L^n)_3$ is favored, complexes with each of the two ligand systems undergo [H^+]-induced ligand dissociation processes via multiple sequential and parallel paths, some of which are common and some of which are different for the two ligands. The pH jump induced ligand dissociation proceeds in two major stages (I and II) where each stage is shown to be comprised of multiple components (I_x, where $x = 1-3$ for L^2 and L^8, and II_y, where $y = 1-3$ for L^2 and $y = 1-4$ for L^8). A reaction scheme consistent with kinetic and independent ESI-MS data is proposed that includes the tris-chelated complexes (coordinated H_2O omitted for clarity) {$Fe_2(L^n)_3$, $Fe_2(L^2)_2(L^2H)_2$, $Fe(L^nH)_3$, $Fe(L^8)(L^8H)$}, bis-chelated complexes {$Fe_2(L^n)_2{}^{2+}$, $Fe(L^nH)_2{}^+$, $Fe(L^8)^+$}, and monochelated complexes {$Fe(L^nH)^{2+}$}. Analysis of kinetic data for ligand dissociation from $Fe_2(L^n)(L^nH)^{3+}$ ($n =$ 2, 4, 6, 8) allows us to estimate the dielectric constant at the reactive dinuclear Fe(III) site. The existence of multiple ligand dissociation paths for the dihydroxamic acid complexes of Fe(III) is a feature that distinguishes these systems from their bidentate monohydroxamic acid and hexadentate trihydroxamic acid counterparts and may be a reason for the biosynthesis of dihydroxamic acid siderophores, despite higher environmental molar concentrations necessary to completely chelate Fe(III).

Introduction

Microbial Fe acquisition is facilitated by the excretion of siderophores, low molecular weight chelators with a high and specific affinity for Fe(III).[1−12] Most siderophores contain hydroxamate, catecholate, and/or α-hydroxycarboxylic acid moieties. The majority of siderophores are hexadentate, where a single ligand can occupy all six Fe(III) coordination sites.[1] Tetradentate siderophores include dihydroxamic acids with linear (e.g., rhodotorulic acid[13,14]) and cyclic structures (e.g., alcaligin[15−17]) as illustrated in Figure 1. Since one dihydroxamic acid ligand cannot saturate all six Fe(III) coordination sites, two or three dihydroxamic acid siderophores must form an assembly with the Fe(III) metal center in a mono- or bimetallic complex.

Thermodynamic solution characterization of the Fe(III)−alcaligin and Fe(III)−rhodotorulic acid complexes has been reported.[14,17] The crystal structure of the alcaligin−Fe(III) complex formed in a 2:3 metal-to-ligand ratio shows a mono-ligand-bridged bimetallic structure, Fe_2L_3.[15] Electrospray ionization mass spectrometry (ESI-MS) shows that in the presence of excess alcaligin ligand the hexachelated mono-Fe(III) species Fe(L)(LH) (see Figure 1 for structural representation) is a major solution component, in addition to Fe_2L_3.[19] A thermodynamic study of the rhodotorulic acid−Fe(III) complex in solution was interpreted in the context of an Fe_2L_3 stoichiometry assumed to have a triply bridged structure,[14] consistent with the crystal structure of a model complex.[18] ESI-MS results show that a

* To whom correspondence should be addressed. E-mail: alc@chem.duke.edu. Fax: 919-660-1605.

(1) Albrecht-Gary, A.-M.; Crumbliss, A. L. In *Iron Transport and Storage in Microoganisms, Plants and Animals*; Sigel, A., Sigel, H., Eds.; Metal Ions in Biological Systems 35; M. Dekker, Inc.: New York, 1998; p 239.
(2) Matzanke, A. F.; Müller-Matzanke, G.; Raymond, K. N. In *Physical Bioinorganic Chemistry Series: Iron Carriers and Iron Proteins*; Loehr, T. M., Ed.; VCH: New York, 1989; p 1.
(3) Crichton, R. R. *Inorganic Biochemistry of Iron Metabolism*; Ellis Horwood: New York, 1991.
(4) Crumbliss, A. L. In *Handbook of Microbial Iron Chelates*; Winkelmann, G., Ed.; CRC Press: Boca Raton, FL, 1991; p 177.
(5) Albrecht-Gary, A.-M.; Crumbliss, A. L. In *Scientific Bridges for 2000 and Beyond*, TEC & DOC editions; Institut de France, Académie des Sciences: Paris, 1999; p 73.
(6) Raymond, K. N.; Telford, J. R. In *Bioinorganic Chemistry: An Inoganic Perspective of Life*; Kessissoglou, D. P., Ed.; NATO ASI Series C: Mathematical and Physical Science 459; Kluwer Acadimic Publishers: Dordrecht, The Netherlands, 1995; p 25.
(7) Raymond, K. N.; Müller, G.; Matzanke, B. F. *Top. Curr. Chem.* **1984**, *123*, 49.
(8) Braun, V.; Hantke, K. In *Transition Metals in Microbial Metabolism*; Winkelmann, G., Carrano, C. J., Eds.; Harwood Academic Publishers: London, U.K., 1997; p 81.
(9) Leong, S. A.; An, Z. In *Transition Metals in Microbial Metabolism*; Winkelmann, G., Carrano, C. J., Eds.; Harwood Academic Publishers: London, U.K., 1997; p 51.
(10) van der Helm, D.; Jalal, M. A. F.; Hossain, M. B. In *Iron Transport in Microbes, Plants and Animals*; VCH Publishers: New York, 1987; p 135.
(11) Biruš, M.; Bradić, Z.; Kujundžić, N.; Pribanić, M. *Prog. React. Kinet.* **1993**, *18*, 173.
(12) Wooldridge, K. G.; Williams, P. H. *FEMS Microbiol. Rev.* **1993**, *12*, 325.
(13) Carrano, C. J.; Cooper, S. R.; Raymond, K. N. *J. Am. Chem. Soc.* **1979**, *101*, 599.
(14) Carrano, C. J.; Raymond, K. N. *J. Am. Chem. Soc.* **1978**, *100*, 5371.
(15) Hou, Z.; Sunderland, C. J.; Nishio, T.; Raymond, K. N. *J. Am. Chem. Soc.* **1996**, *118*, 5148.
(16) Spasojević, I.; Armstrong, S. K.; Brickman, T. J.; Crumbliss, A. L. *Inorg. Chem.* **1999**, *38*, 449.
(17) Hou, Z.; Raymond, K. N.; O'Sullivan, B.; Esker, T. W.; Nishio, T. *Inorg. Chem.* **1998**, *37*, 6630.
(18) Scarrow, R. C.; White, D. L.; Raymond, K. N. *J. Am. Chem. Soc.* **1985**, *107*, 6540.
(19) Spasojević, I.; Boukhalfa, H.; Stevens, R. D.; Crumbliss, A. L. *Inorg. Chem.*, submitted.

10.1021/ic0001659 CCC: $19.00
Published on Web 08/24/2000

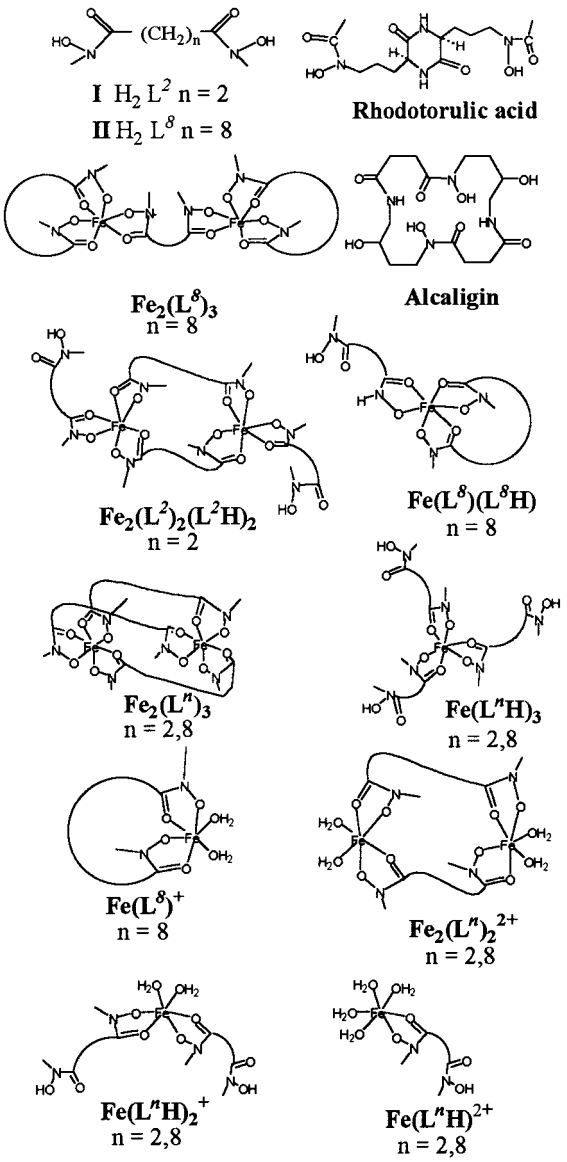

Figure 1. Structural representations for the dihydroxamic acid siderophores acaligin, rhodotorulic acid, the linear synthetic dihydroxamic acids H_2L^n (**I** and **II**), and the structures of their tris-, bis-, and mono(hydroxamato)iron(III) complexes.

monometallic complex (Fe(L)(LH)) is the primary solution species in the presence of excess rhodotorulic acid.[19]

Siderophore-mediated microbial Fe acquisition involves solubilization of environmental iron by selective chelation, transport to the cell by diffusion, molecular recognition, and release of Fe to the cell interior.[1] Iron release involves siderophore−ligand dissociation, and consequently, an understanding of the mechanisms of Fe(III)−siderophore ligand exchange is of importance. This is part of the reason for our current kinetic study, using synthetic linear dihydroxamic acids ($[CH_3N(OH)C{=}O)]_2(CH_2)_n$; L^nH_2; Figure 1) as siderophore models. Additional justification comes from widespread interest in self-assembly mechanisms for polymetallic binding sites and the importance of di-iron centers in biology.

We previously investigated the dissociation kinetics of dihydroxamate ligands (L^nH_2) from their 1:1 Fe(III)/L complexes.[20] The chain length connecting the two hydroxamate groups was the factor that determined whether the 1:1 Fe(III)/L complex was mononuclear (FeL^+) or dinuclear ($Fe_2L_2^{2+}$) at these stoichiometric conditions (throughout this report coordinated H_2O is omitted for clarity). The short connecting chain ($n = 2$ in Figure 1; hereafter designated as H_2L^2) produced the dinuclear species $Fe_2(L^2)_2^{2+}$ (Figure 1), and the long connecting chain ($n = 8$ in Figure 1; hereafter designated as H_2L^8) produced the mononuclear species $Fe(L^8)^+$ at the conditions $[H_2L^n] = [Fe_{aq}^{3+}]$. We now report an extension of that investigation at conditions where $[H_2L^n] > [Fe_{aq}^{3+}]$. We initiate the ligand dissociation process via a pH jump at conditions where Fe(III) is fully chelated by the dihydroxamic acid (i.e., hexacoordinated). ESI-MS experiments show that at the conditions of our kinetic study the fully chelated Fe(III) exists as $Fe(L^2H)_3$, $Fe_2(L^2)_3$, and $Fe_2(L^2)_2(L^2H)_2$ for the short connecting chain ligand L^2H_2 and as $Fe_2(L^8)_3$ and $Fe(L^8)(L^8H)$ for the long connecting chain ligand L^8 (Figure 1).[19] Dissociation of these hexacoordinated tris-chelated complexes produces the tetracoordinated bis-chelated species investigated previously ($Fe(L^8)^+$ and $Fe_2(L^n)_2^{2+}$) as *intermediates*. However, because of the fact that in this study $[H_2L^n] > [Fe_{aq}^{3+}]$, additional bis-chelated species are also present, and therefore, the complete dissociation to Fe_{aq}^{3+} involves more pathways than was observed in our previous study.

Comparing the dissociation kinetics of $Fe_2(L^n)_3$ for L^2H_2 and L^8H_2 in this report addresses reaction path issues related to the structures of the initial and intermediate species that are permitted (or eliminated) as a result of the chain length between the two hydroxamate groups. Tris chelation to form the dinuclear species $Fe_2(L)_3$ can result in a singly or triply ligand bridged structure for H_2L^8, but only a triply ligand bridged structure for H_2L^2 due to steric strain.[20,21] Dissociation of the tris-chelated dinuclear complex provides additional pathways for the L^8 complex, since both mononuclear ($Fe(L^8)^+$) and dinuclear ($Fe_2(L^8)_2^{2+}$) 1:1 Fe/L species are possible as intermediates, whereas only the dinuclear species $Fe_2(L^2)_2^{2+}$ is possible for L^2H_2. Differences in ligand dissociation rates are influenced by the structures of the complexes. Data are presented that are relevant to the effects on the ligand dissociation rates of ligand hydrophobicity, complex stoichiometry, and electrostatic repulsion due to the Fe(III)−Fe(III) distance.

It is the existence of multiple species and multiple reaction paths that distinguishes the ligand exchange reactions of the tetradentate dihydroxamate siderophores from their hexadentate counterparts. These multiple pathways, and the additional lability that they afford the dissociating Fe(III), may play a role in dihydroxamate siderophore mediation of iron bioavailability and may be a rationale for their biosyntheses, despite the higher environmental concentrations required for complete Fe(III) chelation relative to their hexadentate counterparts.

Experimental Section

Materials. All solutions were prepared in deionized water. pH measurements were made using a Corning 250 pH/ion meter equipped with an Orion ROSS pH electrode filled with 3.0 M NaCl solution. The pH was adjusted with NaOH or $HClO_4$ to obtain a neutral solution between 6.5 and 7.5. Stock solutions of 2.0 M $NaClO_4$ were prepared from solid sodium perchlorate hydrate (Aldrich 99+%) and standardized by passing through a Dowex 50 W-X8 strong acid cation exchange column in H^+ form. The 2.0 M $HClO_4$ stock solution was prepared from concentrated perchloric acid (Fisher 70%) and standardized by

(20) Caudle, M. T.; Cogswell, L. P., III.; Crumbliss, A. L. *Inorg. Chem.* **1994**, *33*, 4759.

(21) (a) Caudle, M. T.; Stevens, R. D.; Crumbliss, A. L. *Inorg. Chem.* **1994**, *33*, 843. (b) Caudle, M. T.; Stevens, R. D.; Crumbliss, A. L. *Inorg. Chem.* **1994**, *33*, 6111.

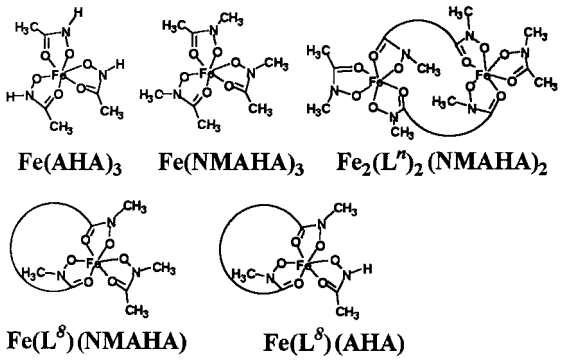

Figure 2. Structures of different tris(hydroxamato)iron(III) complexes, including ternary complexes, where AHA and NMAHA refer to acetohydroxamic acid and *N*-methylacetohydroxamic acid, respectively, and L^n is as defined in Figure 1.

titration with standard NaOH solution to the phenolphthalein end point. Ferric perchlorate stock solution (0.1 M) was prepared from recrystallized ferric perchlorate. It was then standardized spectrophotometrically in strong acid[22] and titrimetrically by reduction with Sn(II) and titrated with the primary standard potassium dichromate.[23]

Ligand and Fe(III) Complex Preparation. Acetohydroxamic acid (AHA) was purchased from Aldrich, and *N*-methylacetohydroxamic acid (NMAHA) was synthesized as described in the literature.[24] The dihydroxamic acid ligands were prepared according to the method described in the literature[25,26] and were recrystallized and characterized as described elsewhere.[20] The tris(hydroxamato)iron(III) complexes were prepared by reacting $Fe(ClO_4)_3$ with the dihydroxamic acid ligand $([CH_3N(OH)C{=}O)]_2(CH_2)_n$ with $n = 2$ (L^2H_2) and $n = 8$ (L^8H_2) carbon chain length between the two hydroxamate units) in 2:3 Fe(III)-to-ligand ratio. The pH was adjusted to neutral (pH = 6.5−7.5) by adding NaOH or $HClO_4$ and the ionic strength adjusted to $I = 2.0$ by $NaClO_4$. The resulting complex turns red and then red-orange at neutral pH. The UV−vis spectra exhibit a strong absorbance characteristic of tris(hydroxamato)iron(III) complexes (λ_{max} at 425 nm, $\epsilon = 2600-2800$ M^{-1} cm^{-1} per Fe).[27] Ternary complexes of NMAHA and AHA with the dihydroxamate ligands L^2 and L^8 (Figure 2) were prepared by adding 1 equiv of the monohydroxamic acid ligand to a solution of the Fe(III) complex that was formed by reacting the dihydroxamate ligand with Fe(III) in a 1:1 Fe/L ratio. The tris(hydroxamato)iron(III) complexes were formed by increasing the pH to neutrality in the presence of L^2 or L^8. All complexes prepared in this way show a strong absorbance as expected for a tris(hydroxamato)iron(III) complex (λ_{max} at 425 nm, $\epsilon = 2600-2800$ M^{-1} cm^{-1} per Fe).

Kinetic Measurements. Ligand dissociation kinetics were performed by mixing tris(hydroxamato)iron(III) complexes at neutral pH with $HClO_4$ of various concentrations (0.0001−1.0 M). Rapid mixing was achieved using an Applied Photophysics stopped-flow instrument (SX.18 MV) equipped with a diode array spectrophotometer with an approximate range of 200−750 nm. All measurements were performed under pseudo-first-order conditions of excess acid at 25 °C and constant ionic strength $I = 2.0$ M ($NaClO_4/HClO_4$). Experimental absorbance decay data were fitted according to the appropriate model using the Applied Photophysics kinetic software. Global analyses were performed on time-dependent spectra using PC Pro-K software (Applied Photophysics).

(22) Bastian, R.; Weberling, R.; Palilla, F. *Anal. Chem*. **1956**, *28*, 459.
(23) Vogel. A. I. *Quantitative Inorganic Analysis Including Elementary Instrumental Analysis*, 3rd ed.; Longmans, Green and Co., Ltd.: London, 1968.
(24) (a) Hauser, C. R.; Renfrow, W. B. *Org. Synth*. **1943**, *2*, 67. (b) Caudle, M. T.; Crumbliss, A. L. *Inorg. Chem*. **1994**, *33*, 4077.
(25) Smith, W. L.; Raymond, K. N. *J. Am. Chem. Soc*. **1980**, *102*, 1252.
(26) Das, M. K.; Roy, N. *J. Chem. Eng. Data* **1984**, *29*, 345.
(27) Barclay, S.; Huynh, H. B.; Raymond, K. N. *Inorg. Chem*. **1984**, *23*, 2011.

Results

General Observations. For simplicity, the complexes formed with the dihydroxamate ligands **I** and **II** (Figure 1) with the two hydroxamate units separated by two methylene groups and eight methylene groups are noted as L^2H_2 and L^8H_2, respectively. The ternary complexes formed by adding *N*-methylacetohydroxamic acid (NMAHA) and acetohydroxamic acid (AHA) ligands to the bis(hydroxamato)iron(III) complexes of L^2 and L^8 are designated $(NMAHA)_2Fe_2(L^n)_2$, $(AHA)_2Fe_2(L^n)_2$, (NMAHA)Fe(L^8), and (AHA)Fe(L^8), respectively (Figure 2). Throughout this report coordinated H_2O is omitted for clarity.

All tris(hydroxamato)iron(III) complexes studied yield a red-orange solution at neutral pH with an absorbance maximum at 425 nm. In more acidic media (pH = 2), the solutions turn red with an absorbance maximum at 470 nm ($\epsilon_{bis} = 1750-1850$ M^{-1} cm^{-1} per Fe), which is attributed to the bis(hydroxamato)iron(III) complexes $Fe(L^n)^+$ and $Fe_2(L^n)_2{}^{2+}$. As the pH is lowered to more acidic media (pH < 1), the absorbance maximum is shifted to a longer wavelength, $\lambda_{max} = 500$ nm, for complexes with L^2. The L^8 complexes do not show displacement of the absorbance maximum above 470 nm. These general spectral changes are the result of changing the number of ligating hydroxamate groups at the Fe(III) center and are in good agreement with known spectral characteristics of Fe(III)−hydroxamate complexes.[27]

Mixing trishydroxamate-chelated Fe(III) complexes with $HClO_4$ at various concentrations (0.0001−1.0 M) results in different degrees of hydroxamate group dissociation in a multistep time-dependent process. Independent ESI-MS experiments establish that under our conditions of full Fe(III) chelation the following hexacoordinate species are present: $Fe(L^2H)_3$, $Fe_2(L^2)_3$, and $Fe_2(L^2)_2(L^2H)_2$ for the dihydroxamate ligand L^2; and $Fe_2(L^8)_3$ and $Fe(L^8)(L^8H)$ for the dihydroxamate ligand L^8.[19] H^+-jump experiments in a moderate acidity range ($[H^+] = 0.0001-0.06$ M) were carried out under conditions where the Fe(III) coordination sites were completely saturated by hydroxamate coordination. This enabled us to analyze kinetic data associated with stage I of the ligand dissociation process, which occurs in three distinct steps (labeled I_x, where *x* designates step 1, 2, or 3). Spectral shifts for stage I ($[H^+] = 0.0001-0.06$ M) correspond to the tris-chelated Fe(III) complex dissociating to the bis-chelated Fe(III) species. Higher acidity H^+ jump experiments ($[H^+] = 0.1-1.0$ M) permitted us to analyze stage II of the ligand dissociation process, which is also a multistep process (labeled II_y where *y* designates steps 1−3 for L^2 and 1−4 for L^8). Spectral shifts for stage II correspond to the complete dissociation of the bis-chelated complex to give the aquated ferric ion, $Fe_{aq}{}^{3+}$. Figure 3 shows the overall absorbance decay recorded during the acid dissociation of the complexes with L^2 and L^8, respectively.

Stage I. Tris(hydroxamato)iron(III) Dissociation. Time-dependent spectral changes on mixing H^+ ($[H^+] = 0.0001-0.06$ M) with trishydroxamate-chelated Fe(III) are similar for both the L^2 and L^8 complexes. Fast absorbance decay on a 15 ms time scale is observed for both L^2 and L^8 complexes (parts A and B of Figure 3).

During the first fast step a decrease in absorbance intensity and shift in the absorbance maximum to longer wavelength ($\lambda_{max} = 460$ nm) are observed. The total absorbance change increases with increasing $[H^+]$. The proton stoichiometry for the fast process (I_1) was determined by analyzing the final absorbance (at 15 ms) according to

$$Fe(L^nH)_3 + H^+ \rightleftharpoons Fe(L^nH)_2{}^+ + H_2L^n, \quad K_9, k_9, k_{-9} \quad (1)$$

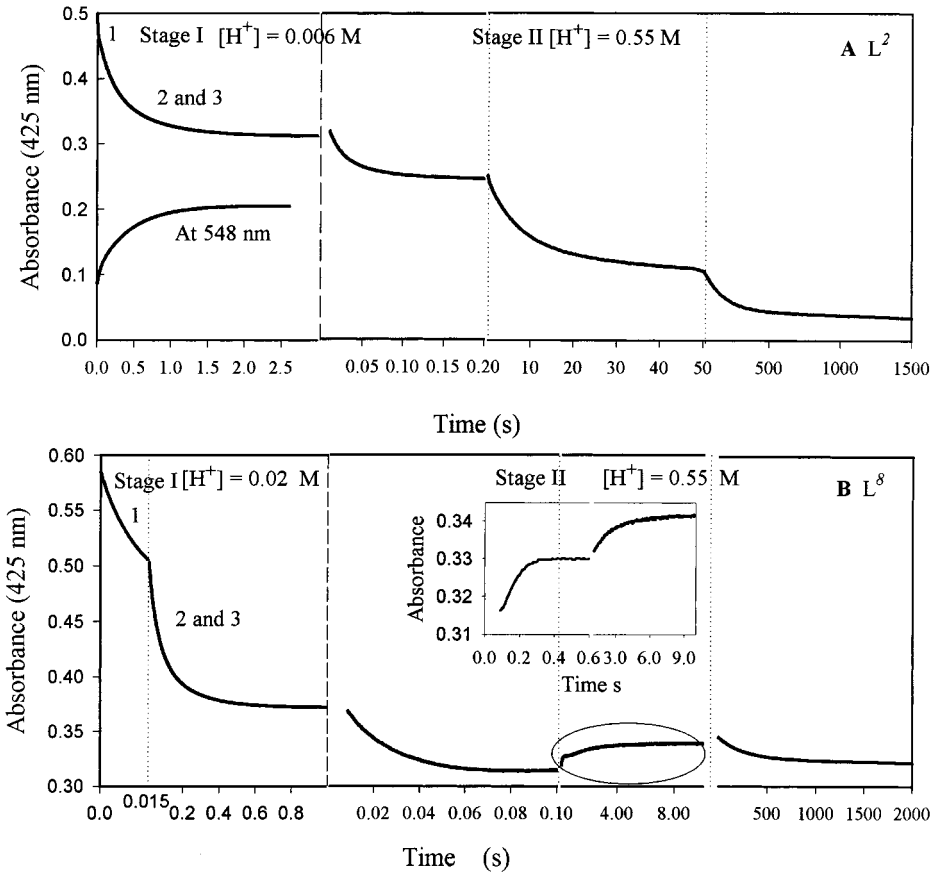

Figure 3. Overall absorbance decay for the H^+-initiated ligand dissociation of the tris(hydroxamato)iron(III) complex with ligands L^2 (A) and L^8 (B). Conditions are the following: $[Fe^{3+}]_{tot} = 0.2$ mM; $[L^nH_2]_{tot} = 0.3-0.4$ mM; $I = 2.0$ M ($NaClO_4/HClO_4$); $T = 25$ °C; $\lambda = 425$ and 548 nm; (A) $[H^+] = 0.006$ and 0.55 M for stage I and stage II, respectively; (B) $[H^+] = 0.02$ and 0.55 M for stage I and stage II, respectively.

where $L^n = L^2$ or L^8. Reaction 1 is considered as a quasi-equilibrium where the following step does not proceed to any significant degree. Equation 2,

$$Abs_{eq} = \frac{(Abs_i - Abs_{eq})[H_2L^n]}{K_9[H^+]} + Abs_{fin} \qquad (2)$$

relates the H^+-dependent quasi-equilibrium absorbance (Abs_{eq}) (reaction 1) to the initial absorbance (Abs_i), final absorbance after reaction 1 (end of stage I_1; Abs_{fin}), and total ligand $[H_2L^n]$ and $[H^+]$ concentrations. A linear plot obtained by assuming one H^+ is involved is in good agreement with reaction 1 (see Figure 4A, data for $Fe(L^2H)_3$). At various H^+ concentrations the apparent dissociation rate constant for the first dissociation reaction (I_1) was determined by numerical fitting of the signal by the monoexponential equation

$$A - Abs_{eq} = B\exp(-k_9^{obs}t) \qquad (3)$$

on a 15 ms time scale. The dissociation rate of $Fe(L^nH)_3$ in reaction 1, assuming a constant ligand concentration, is represented by the differential equation:

$$-\frac{d([Fe(L^nH)_3])}{dt} = (k_9[H^+] + k_{-9}[H_2L^n])([Fe(L^nH)_3] - [Fe(L^nH)_3]_\infty) \qquad (4)$$

Integration of eq 4 gives the apparent rate constant k_9^{obs}:

$$k_9^{obs} = k_9[H^+] + k_{-9}[H_2L^n] \qquad (5)$$

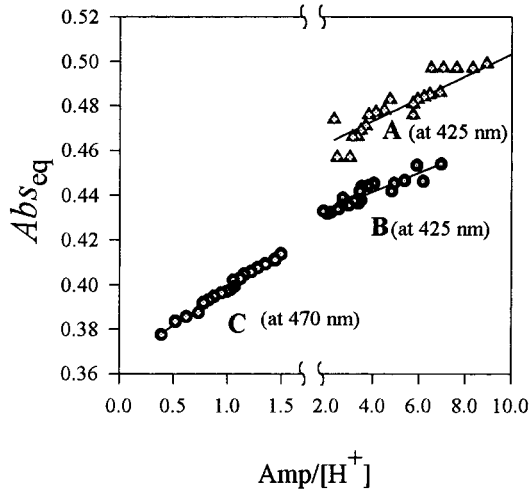

Figure 4. Absorbance data at 425 and 470 nm collected at the quasi-equilibrium position after stage I_1 (A), stage I_2 (B), and stage II_1 (C) for the Fe(III)/L^2 system plotted as a function of absorbance amplitude times $[H^+]^{-1}$. Solid lines represent the linear regression $Abs_{eq} = a/[H^+] + Abs_{fin}$ (see eq 2). Conditions are the following: $[L^2H_2]_{tot} = 0.3$ mM, $[Fe_{aq}^{3+}]_{tot} = 0.2$ mM; $I = 2.0$ M ($NaClO_4/HClO_4$); $T = 25$ °C; (A) $[H^+] = 0.0001-0.06$ M, $a = 5.02 \times 10^{-3}$, $Abs_{fin} = 0.453$ ($R^2 = 0.81$); (B) $[H^+] = 0.0001-0.06$ M, $a = 4.24 \times 10^{-3}$, $Abs_{fin} = 0.424$ ($R^2 = 0.85$); (C) $[H^+] = 0.1-1.0$ M, $a = 0.032$, $Abs_{fin} = 0.366$ ($R^2 = 0.98$).

A plot of k_9^{obs} vs $[H^+]$ shows linear behavior (Figure 5). Values of k_9 (Table 1) were obtained from a linear fit of eq 5 to the experimental data. The intercepts in Figure 5 are not precise, and no accurate value is obtained for k_{-9}.

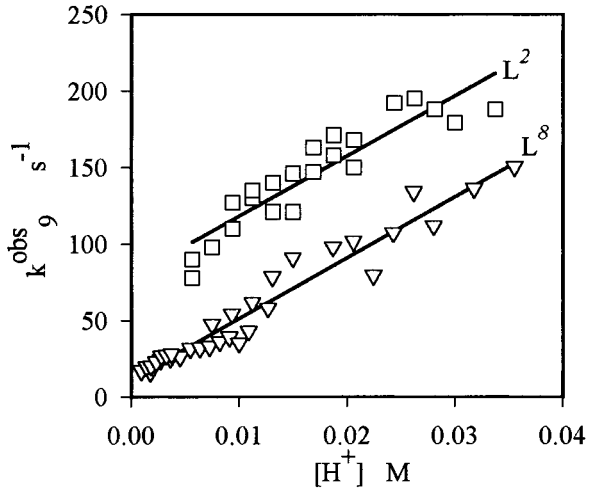

Figure 5. Stage I_1 kinetic data for the acid dissociation of the tris(hydroxamato)iron(III) complex $Fe(L^nH)_3$ ($n = 2$ (□), $n = 8$ (▽)) showing observed pseudo-first-order rate constant (k_9^{obs}) for reaction 1 plotted as a function of $[H^+]$. Conditions are the following: $[Fe^{3+}]_{tot} = 0.2$ mM; $[L^nH_2]_{tot} = 0.3$ mM; $I = 2.0$ M ($NaClO_4/HClO_4$); $T = 25$ °C; $\lambda = 425$ nm. Solid line represents the linear regression $k_9^{obs} = a[H^+] + b$ (see eq 5). (□) $a = 3923(382)$ M^{-1} s^{-1}, $b = 79(7)$ s^{-1}, $R^2 = 0.84$. (▽) $a = 3974(172)$ M^{-1} s^{-1}, $b = 12$ (3) s^{-1}, $R^2 = 0.94$. Numbers in parentheses represent the standard error.

Table 1. Microscopic Kinetic Parameters[a] Defined in Schemes 1−3 for the Dissociation of Tris- and Bis(dihydroxamato)iron(III) Complexes

		values (standard deviation)	
reaction no.	parameters	L^2	L^8
1	k_9, M^{-1} s^{-1}	3923(382)	3974(172)
7	K_{12}, M^{-1}	442(236)	207(54)
8	k_8, M^{-1} s^{-1}	1828(38)	1495(22)
8	k_{-8}, s^{-1}		0.014(0.005)
11, 12	k_{10}, M^{-1} s^{-1}	422.6(4)	284(10)
13	k'_{10}, M^{-1} s^{-1}		316(6)
14	k''_{10}, M^{-1} s^{-1}	481(14)	
17, 26	k_7, M^{-1} s^{-1}	91.9(3)	65.2(1.5)
17, 26	k_{-7}, M^{-1} s^{-1}	141(5)	9.7(0.9)
18, 29	K_4, M^{-1}	0.9(0.35) 0.6[b]	0.81(0.4)
19, 30	k_3, M^{-1} s^{-1}	1.33(0.3) 1.6[b]	30.17(6)
19, 30	k_{-3}, M^{-1} s^{-1}	0.017(0.008) 0.016[b]	0.2(0.2)
24	k_1, M^{-1} s^{-1}	0.0019[b]	0.0016(2 × 10^{-4}) 0.0008[b]
24	k_{-1}, M^{-1} s^{-1}	1.6[b]	40[b]
25	k'_1, s^{-1}	0.0069[b]	0.00056(3 × 10^{-5}) 0.00055[b]
25	k'_{-1}, M^{-1} s^{-1}	3.8[b]	18[b]
27	k_5, M^{-1} s^{-1}		16.2(0.85) 17[b]
27	k_{-5}, s^{-1}		11.2(0.43) 10[b]
28	k_6, s^{-1}		0.13(0.04)[b]

[a] Conditions are as described in figure captions and text. [b] Reference 20.

The very fast step (I_1) is followed by a biexponential absorbance decay whose two components are referred to as stages I_2 and I_3 (Figure 3). The dissociation reactions were monitored at 425 and 548 nm on a time scale of 0.015−20 and 0.015−2 s, respectively, depending on the H^+ concentration. The signal at 548 nm was observed as an increase in absorbance, since the spectral changes exhibit an isosbestic point at $\lambda =$ 470 nm. Data recorded at 548 nm were more suitable for numerical fitting, since further reaction in the following stage shows an isosbestic point at $\lambda = 548$ nm and prevents the overlapping of the two absorbance decays. The apparent rate constants were determined by fitting the absorbance change at 548 nm as a biexponential signal according to

$$\mathrm{Abs} - \mathrm{Abs}_{eq} = B\exp(-k_8^{obs}t) + C\exp(-k_{10}^{obs}t) \qquad (6)$$

where B and C are the amplitudes. Spectral changes are consistent with tris(hydroxamato)iron(III) dissociating to a bis(hydroxamato)iron(III) complex (Supporting Information, Figure S1). Close analysis of the data shows that as the ligand dissociation proceeds, a shift from isosbestic behavior is observed. The final absorbance maximum is shifted to longer wavelength ($\lambda_{max} = 470$ nm). The spectral changes may be separated into two sets of spectra, where the first set exhibits an isosbestic point at $\lambda = 470$ nm with an absorbance maximum shifted from 430 to 470 nm. The second set of spectra give an isosbestic point at $\lambda = 495$ nm, and the absorbance maximum is also shifted from 430 to 470 nm. These time-resolved spectral data are interpreted as arising from two parallel ligand dissociation reactions resulting from the dissociation of tris(hydroxamato)iron(III) complexes having different structures.

The first of these spectral changes (stage I_2) is attributed to the dissociation of the bimetallic triply bridged complex Fe_2L_3 according to

$$Fe_2(L^n)_3 + H^+ \rightleftharpoons Fe_2(L^n)_2(L^nH)^+ \quad K_{12} \qquad (7)$$

and

$$Fe_2(L^n)_2(L^nH)^+ + H^+ \rightleftharpoons Fe_2(L^n)_2^{2+} + H_2L^n \quad K_8, k_8, k_{-8} \qquad (8)$$

Reaction 7 represents a rapid preequilibrium followed by a relatively slow dissociation step (eq 8). Both L^2 and L^8 complexes show a nonlinear dependence of the apparent dissociation rate with respect to H^+ concentration (Figure 6). The proposed scheme in eqs 7 and 8 is based on the observed second-order $[H^+]$-dependent kinetics. The amplitude of the absorbance change associated with stage I_2 computed from a numerical fitting of the absorbance decay according to eq 6 and plotted according to eq 2 gives a linear plot for one H^+ (Figure 4 B). However, this is due to the fact that the two metal centers in the bimetallic complex are equivalent; therefore, we cannot distinguish between protonation at either center, and the overall observed absorbance change is that due to the protonation of one Fe(III) center involving a single H^+. The same result was reported for this system when studying the dissociation of the bimetallic complex $Fe_2(L^2)_2^{2+}$.[20] Consideration of rapid equilibrium reaction 7 followed by reaction 8 yields the differential rate equation

$$-\frac{d[Fe_2(L^n)_3]}{dt} = \left(\frac{k_8K_{12}[H^+]^2}{1 + K_{12}[H^+]} + k_{-8}[H_2L]\right)([Fe_2(L^n)_3] - [Fe_2(L^n)_3]_\infty) \qquad (9)$$

Making the valid assumption that the free ligand concentration

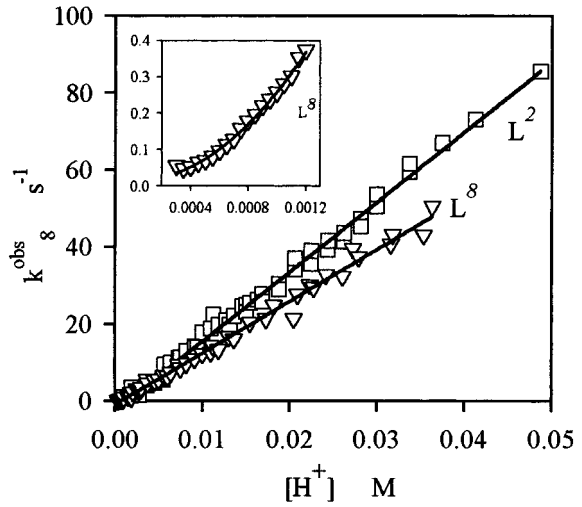

Figure 6. Stage I_2 kinetic data for the acid dissociation of the tris(hydroxamato)iron(III) complex (L^2 (□) and L^8 (▽)). Observed pseudo-first-order rate constant (k_8^{obsd}) for reaction 8 plotted as a function of [H^+]. Conditions are the following: $[Fe^{3+}]_{tot}$ = 0.2 mM; $[H_2L^n]_{tot}$ = 0.3 mM; I = 2.0 M ($NaClO_4/HClO_4$); T = 25 °C; λ = 548 nm. Solid lines represent the regression $k_8^{obs} = a[H^+]^2/(1 + b[H^+]) + c$ (see eq 10). (□) $a = 1.828 \times 10^3$ (38), b = 462(236), c = 0.46(0.5), R^2 = 0.99. (▽) $a = 1.495 \times 10^3$ (22), b = 207(54), c = 0.28(0.4), R^2 = 0.98. The numbers in parentheses represent the standard error.

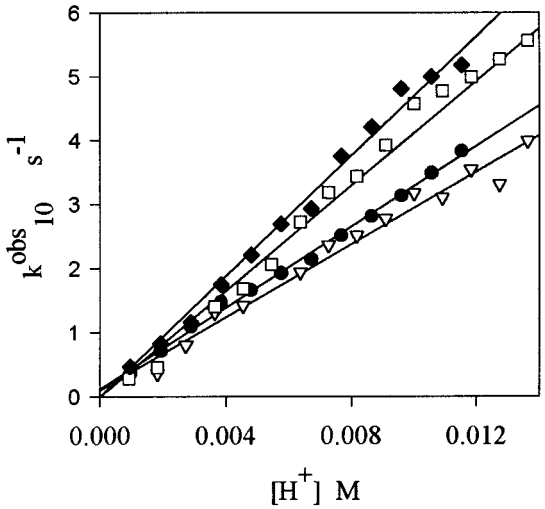

Figure 7. Stage I_3 kinetic data for the acid dissociation of the tris(hydroxamato)iron(III) complexes $Fe(L^8)(L^8H)$ (▽) and $Fe_2(L^2)_2(L^2H)_2$ (□) and ternary complexes $Fe_2(L^2)_2(NMAHA)_2$ (◆) and $Fe(L^8)(NMAHA)$ (●). Observed pseudo-first-order rate constant (k_{10}^{obs}, $k_{10}^{obs\prime}$, or $k_{10}^{obs\prime\prime}$) for reactions 11, 12, 13, or 14 plotted as a function of [H^+]. Conditions are the following: $[Fe^{3+}]_{tot}$ = 0.2 mM; $[H_2L^n]_{tot}$ = 0.3 mM; I = 2.0 M ($NaClO_4/HClO_4$); T = 25 °C; λ = 548 nm. Solid lines represent the linear regression $k_{10}^{obs} = a[H^+] + b$ (see eq 16). (□) a = 412(4) M^{-1} s^{-1}, b = 0(0.07), R^2 = 0.98. (◆) a = 481(14) M^{-1} s^{-1}, b = 0 (0.1), R^2 = 0.98. (▽) a = 284(10) M^{-1} s^{-1}, b = 0.1(0.12), R^2 = 0.98. (●) a = 316(6) M^{-1} s^{-1}, b = 0(0.05), R^2 = 0.98. The numbers in parentheses represent the standard error.

is small and constant, integration of eq 9 gives the apparent dissociation rate constant k_8^{obs}:

$$k_8^{obs} = \frac{k_8 K_{12}[H^+]^2}{1 + K_{12}[H^+]} + k_{-8}[H_2L] \qquad (10)$$

Values for k_8 (Table 1) are obtained by fitting eq 10 to the data presented in Figure 6. The intercept is small, and no accurate value was obtained to define k_{-8} for the L^2 complex.

The third dissociation reaction (stage I_3) is attributed to the dissociation of the $Fe_2(L^2)_2(L^2H)_2$ species for the L^2 complexes and to $Fe(L^8)(L^8H)$ for the L^8 complexes. The corresponding ligand dissociation reactions are

$$Fe(L^8)(L^8H) + H^+ \rightleftharpoons Fe(L^8)^+ + H_2L^8 \quad K_{10}, k_{10}, k_{-10} \qquad (11)$$

and

$$Fe_2(L^2)_2(L^2H)_2 + H^+ \rightleftharpoons Fe_2(L^2)_2(L^2H)^+ + H_2L^2 \quad K_{10}, k_{10}, k_{-10} \qquad (12)$$

A linear dependence of the apparent dissociation rates vs [H^+] concentration is observed (Figure 7), and the resulting rate parameters are listed in Table 1.

Ternary Complex Dissociation. A series of ternary complexes (Figure 2) of equivalent structure were prepared in situ to confirm the above interpretation of the stage I_3 kinetic data. One equivalent of NMAHA or AHA was added to the complex formed in 1:1 Fe/L^n ratio to form $(NMAHA)_2Fe_2(L^2)_2$ for L^2 and $(NMAHA)Fe(L^8)$ and $(AHA)Fe(L^8)$ for L^8, as evidenced by their λ_{max} at 425 nm. Reaction of the ternary complexes with H^+ ([H^+] = 0.001−0.06 M) results in a monoexponential absorbance decay and λ_{max} shift to longer wavelength (λ_{max} = 470 nm; ϵ = 1750−1850 M^{-1} cm^{-1}), consistent with ligand dissociation to produce a bis(hydroxamato)Fe(III) complex. The apparent dissociation rates determined by numerical fitting of the absorbance change by a monoexponential equation show first-order dependence on H^+ concentration. The corresponding dissociation reactions are described in

$$Fe(L^8)(L') + H^+ \rightleftharpoons Fe(L^8)^+ + HL', \quad (K'_{10}, k'_{10}, k'_{-10}) \qquad (13)$$

and

$$Fe_2(L^2)_2(L')_2 + H^+ \rightleftharpoons Fe_2(L^2)_2(L')^+ + HL', \quad K''_{10}, k''_{10}, k''_{-10} \qquad (14)$$

where HL′ = NMAHA and AHA.

Equation 15 (shown for the specific case of reaction 11) gives the general form of the differential rate equation corresponding to reactions 11−14. The apparent dissociation rate constant k_{10} (k'_{10} and k''_{10}) is derived by integration of the differential equation

$$-\frac{d[Fe(L^8)(L^8H)]}{dt} = (k_{10}[H^+] + k_{-10}[H_2L^8])([Fe(L^8)(L^8H)]_0 - [Fe(L^8)(L^8H)]_\infty) \qquad (15)$$

when the ligand concentration is constant to give

$$k_{10}^{obs} = k_{10}[H^+] + k_{-10}[H_2L^8] \qquad (16)$$

Data in Figure 7 represent a plot of k_{10}^{obs} (k'_{10} and k''_{10}) vs [H^+]. The rate constants k_{10} and k_{-10} were determined from a linear fit of eq 16 to the data as shown in Figure 7 (Table 1). The ligand dissociation rate constant for the ternary complex $(NMAHA)_2Fe_2(L^2)_2$ is equivalent to the dissociation rate constant attributed to the species $Fe_2(L^2)_2(L^2H)_2$, and the dissociation rate constant for the ternary complex (NMAHA)-$Fe(L^8)$ is equivalent to that observed for $Fe(L^8)(L^8H)$ (Figure

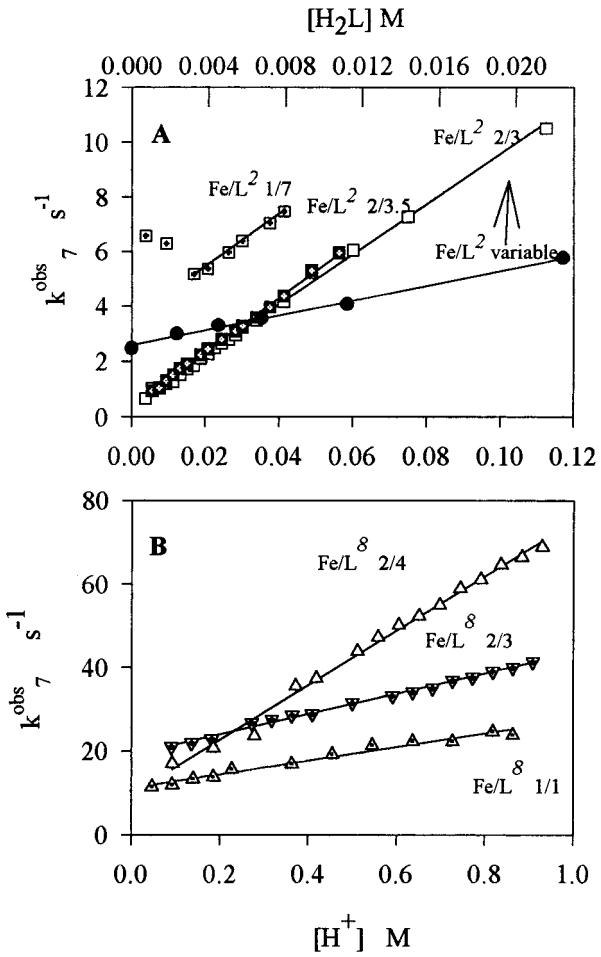

Figure 8. Stage II_1 kinetic data for the acid dissociation of the bis(hydroxamato)iron(III) complexes with L^2 (A) and L^8 (B). Observed pseudo-first-order rate constant (k_7^{obs}) plotted as a function of $[H^+]$ for reactions 17 and 26 at different Fe/L^n ratios. Conditions are the following: $[Fe^{3+}]_{tot} = 0.2$ mM; $[H_2L^n]_{tot}$ varied to achieve the final Fe/L^n ratio; $I = 2.0$ M ($NaClO_4/HClO_4$); $T = 25$ °C; $\lambda = 570$ nm. Solid line represents the linear regression $k_7^{obs} = a[H^+] + b$ (see eq 21). (A) Fe/L^2 = $^2/_3$, $a = 91.9(1)$ M^{-1} s^{-1}, $b = 0.38(0.04)$ s^{-1}, $R^2 = 0.997$; Fe/L^2 = $^2/_{3.5}$, $a = 98.5(1.2)$ M^{-1} s^{-1}, $b = 0.37(0.04)$ s^{-1}, $R^2 = 0.998$; Fe/L^2 = $^1/_7$, $a = 95.88(3)$, $b = 3.5(0.1)$, $r^2 = 0.995$; (●) dissociation kinetics at fixed H^+ concentration $[H^+] = 0.022$ M and variable $[H_2L^2]$, Fe/L^2 (top scale) < $^2/_3$, $a = 141(5)$ M^{-1} s^{-1} and $b = 2.6(0.1)$ s^{-1}, $R^2 = 0.995$. (B) Fe/L^8 = $^2/_4$, $a = 65.2(1.5)$ M^{-1} s^{-1}, $b = 9.7(0.9)$ s^{-1}; Fe/L^8 = $^2/_3$, $a = 24.16(0.5)$ M^{-1} s^{-1}, $b = 19.2(0.3)$ s^{-1}, $R^2 = 0.994$; Fe/L^8 = 1/1, $a = 16.2(0.8)$ M^{-1} s^{-1}, $b = 11.2(0.4)$ s^{-1}, $R^2 = 0.974$. The numbers in parentheses represent the standard error.

7, Table 1). This confirms our mechanistic interpretation of the stage I_3 kinetic data.

Stage II. General Observations. Contrary to the behavior observed for stage I, the L^2 and L^8 complexes exhibited divergent behavior in stage II. Ligand dissociation kinetics in stage II ($[H^+] = 0.1-1.0$ M) for the L^2 complex shows three successive first-order absorbance decays occurring at 0.2, 50, and 1500 s for stage II_y, $y = 1, 2, 3$, respectively. The L^8 complex, over the same acid concentration range, exhibits a first-order absorbance decay, followed by two first-order absorbance *increases*, followed by a slow absorbance decay, with the corresponding time scales of 0.1, 0.4, 10, and 2000 s (stage II_y, $y = 1, 2, 3, 4$, respectively). These observations are illustrated in Figure 3.

Stage II. L^2 Complex. The time-dependent absorbance decays observed during stage II were monitored at 470 nm. The

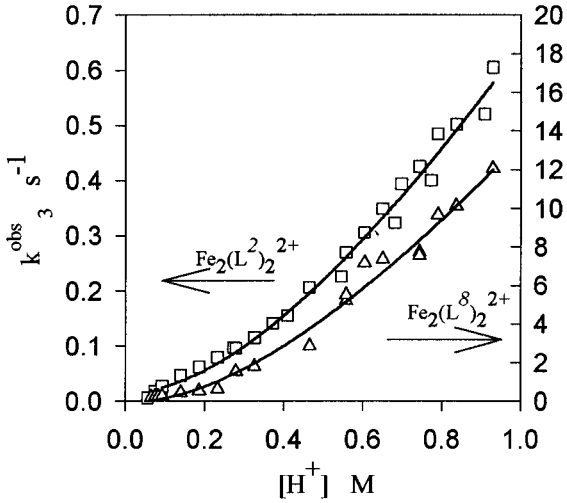

Figure 9. Stage II_2 kinetic data for the acid dissociation of bis(hydroxamato)iron(III) complexes $Fe_2(L^2)_2^{2+}$ (□) and $Fe_2(L^8)_2^{2+}$ (△). Observed pseudo-first-order rate constant k_3^{obsd} plotted as a function of $[H^+]$ for reactions 18, 19 and 29, 30. Conditions are the following: $[Fe^{3+}]_{tot} = 0.2$ mM; $[H_2L^n]_{tot} = 0.3$; $I = 2.0$ M ($NaClO_4/HClO_4$); $T = 25$ C; $\lambda = 470$ nm. Solid line represents regression analysis of the data according to the equation $k_3^{obs} = a[H^+]^2/(1+ b[H^+]) + c$ (see eq 23). For $Fe_2(L^2)_2^{2+}$ (□) $a = 1.2$ (0.2) M^{-1} s^{-1}, $b = 0.9(0.35)$, $c = 0.002$-(0.001), $R^2 = 0.989$. $Fe_2(L^8)_2^{2+}$ (▽) $a = 24.44(6)$ M^{-1} s^{-1}, $b = 0.81$-(0.4), $c = -0.004(0.005)$, $R^2 = 0.984$. The numbers in parentheses represent the standard error.

time-dependent spectra recorded during the first absorbance decay (stage II_1) show an isosbestic point at 548 nm with λ_{max} shifted above 470 nm (Supporting Information, part A of Figure S2). This behavior is consistent with the dissociation of a bis(hydroxamato)iron(III) complex. Spectral changes in stage II_2 show the same behavior with an isosbestic point at 548 nm (Supporting Information, part B of Figure S2) and are also consistent with the dissociation of a bis(hydroxamato)iron(III) complex. Kinetic data determined from separately fitting the first two absorbance decays with a monoexponential equation show first-order H^+ dependence for the first step (stage II_1, Figure 8A) and second-order H^+ dependence for the second step (stage II_2, Figure 9).

These data are consistent with a parallel scheme in which two different reactants dissociate to give the same product. The first process is attributed to the dissociation of $Fe(L^2H)_2^+$ involving one H^+ according to

$$Fe(L^2H)_2^+ + H^+ \rightleftharpoons Fe(L^2H)^{2+} + H_2L^2 \quad (K_7, k_7, k_{-7}) \quad (17)$$

A parallel second-order H^+-dependent dissociation reaction is attributed to the dissociation of the bimetallic species $Fe_2(L^2)_2^{2+}$ according to

$$Fe_2(L^2)_2^{2+} + H^+ \rightleftharpoons Fe_2(L^2)(L^2H)^{3+} \quad K_4 \qquad (18)$$

and

$$Fe_2(L^2)(L^2H)^{3+} + H^+ \rightleftharpoons 2Fe(L^2H)^{2+} \quad K_3, k_3, k_{-3} \qquad (19)$$

The reaction stoichiometry for eq 17 was confirmed by plotting the final absorbance according to the Schwarzenbach equation, where a linear plot is obtained for one H^+ (Figure 4C). The dissociation rate of the complex $Fe(L^2H)_2^+$ according to reaction 17 is expressed by the differential equation

$$-\frac{d([Fe(HL^2)_2^+])}{dt} = (k_7[H^+] + k_{-7}[H_2L^2])([Fe(HL^2)_2^+] - [Fe(HL^2)_2^+]_\infty) \quad (20)$$

Integration of eq 20 considering a small and constant ligand concentration yields the apparent rate constant k_7^{obs}:

$$k_7^{obs} = k_7[H^+] + k_{-7}[H_2L^2] \quad (21)$$

The apparent dissociation rate constant k_7^{obs} is found to be both ligand- and proton-dependent as illustrated in Figure 8. The slope of the plot of k_7^{obs} vs $[H^+]$ is not sensitive to variations in free ligand concentration, but the intercept increases with an increase in free ligand concentration. The ligand dependence of this step in the overall reaction was probed by performing dissociation kinetics at constant $[H^+]$ at different $[L^2H_2]$. At fixed $[H^+]$ the apparent dissociation rate constant k_7^{obs} shows a linear dependence with respect to ligand concentration (see Figure 8A, upper axis). The rate constants k_7 and k_{-7} (Table 1) were obtained from a linear fit of eq 21 to the experimental data in the H^+- and ligand-dependent experiments, respectively.

The apparent dissociation rate of the bis(hydroxamato)iron(III) complex $Fe_2(L^2)_2^{2+}$ according to reactions 18 and 19 is given by the differential equation

$$-\frac{d[Fe_2(L^2)_2^+]}{dt} = \left(\frac{k_3K_4[H^+]^2}{1 + K_4[H^+]} + 2k_{-3}\right)([Fe_2(L^2)_2^+] - [Fe_2(L^2)_2^+]_\infty) \quad (22)$$

by assuming that reaction 18 is a fast preequilibrium to reaction 19. The apparent pseudo-first-order rate constant is expressed by

$$k_3^{obs} = \frac{k_3K_4[H^+]^2}{1 + K_4[H^+]} + 2k_{-3} \quad (23)$$

by assuming low and constant ligand concentration. The apparent rate constant exhibits a second-order dependence on proton concentration as seen in Figure 9. The values of k_3, k_{-3}, and K_4 (Table 1) were obtained by fitting eq 23 to the experimental data. The kinetic parameters determined for the $Fe_2(L^2)_2^{2+}$ path are in good agreement with the values from the previous investigation[20] performed for the complex of this stoichiometry prepared at pH 2 in a 1:1 Fe/L ratio (Table 1).

The kinetic data for the successive dissociation of $Fe(L^2H)_2^+$ and $Fe_2(L^2)_2^{2+}$ are in good agreement with the mechanism proposed in stage I, since the two bis(hydroxamato)iron(III) complexes are the products of the dissociation of the species involved in stage I. In our previous study,[20] conducted at a 1:1 Fe/L^2 ratio, the species $Fe(L^2H)_2^+$ was not observed. We confirmed this by performing our L^2 ligand dissociation study at 1:1 Fe/L^2 conditions with results similar to the previous study. This demonstrates that the species $Fe(L^2H)_2^+$ is the result of the dissociation of $Fe(L^2H)_3$ formed in 2:3 Fe/L^2 and higher ligand concentrations.

The third dissociation step (stage II_3) was observed at 470 nm as a monoexponential absorbance decay. The time-dependent spectral changes during the slow step are consistent with ligand dissociation from the mono(hydroxamato)iron(III) complex to give aquated Fe(III). The overall absorbance decreases without a significant shift of the absorbance maximum above 500 nm (Supporting Information, part C of Figure S2). Kinetic data for the slow dissociation are not presented because the results are as expected and similar to the slow step observed in our previous study conducted at a 1:1 Fe/L^2 metal-to-ligand ratio.[20] The Fe-$(L^2H)^{2+}$ dissociation was interpreted as a relaxation reaction mechanism according to

$$Fe(L''H)^{2+} + H^+ \rightleftharpoons Fe(H_2O)_6^{3+} + H_2L'' \quad K_1, k_1, k_{-1} \quad (24)$$

$$Fe(L''H)^{2+} \rightleftharpoons FeOH(H_2O)_5^{2+} + H_2L'' \quad K_1', k_1', k_{-1}' \quad (25)$$

(H^+ $\rightleftharpoons$ K_h)

The rate constants k_1, k_{-1}, k'_1, and k'_{-1} are summarized in Table 1.

Stage II. L^8 Complex. Absorbance changes observed during stage II for the L^8 complex were monitored at 470 nm where ligand dissociation from the tris(hydroxamato)iron(III) complex does not interfere. A mono-exponential decay was observed on a time scale of 0.1 s. The amplitude of the absorbance decay is more significant for the complex formed at >2:3 Fe/L^8 ratios than for the complexes formed under the conditions where the Fe/L^8 ratio equals 2:3. The reaction stoichiometry was determined from a plot of the absorbance at the end of the stage II_1 absorbance decay according to the Schwarzenbach relationship shown in eq 2. A linear plot was obtained for a single stoichiometric H^+ (data not shown). The overall time-dependent spectra recorded in the 0.1 s time frame for the complex prepared in a 2:4 Fe/L ratio (Supporting Information, part A of Figure S3) exhibit the same characteristics as observed for stage II_1 for the L^2 complex (Supporting Information, part A of Figure S2). However, for the complex prepared in 1:1 Fe/L^8 ratio this step is not observed and the overall time-dependent spectra show a decrease of the absorbance over all wavelengths (Supporting Information, part B of Figure S3). Spectral changes are attributed to the L^8 ligand dissociation from a bis(hydroxamato)iron(III) complex. The L^8 ligand with a long carbon chain (eight $-(CH_2)-$ groups) forms bis(hydroxamato)iron(III) complexes of different structures; $Fe_2(L^8)_2^{2+}$, $Fe(L^8)^+$, and $Fe(L^8H)_2^+$ are bis complexes to be considered at the conditions where the Fe/L ratio is 2:3 (see Figure 1).

Kinetic data for ligand dissociation performed at the conditions where the Fe/L^8 ratio was 1:1 exhibited first-order dependence of the apparent dissociation rate constant with respect to $[H^+]$. The dissociation of the complex performed by adding excess L^8 ligand in the acidic solution did not affect the dissociation rate. However, when the complex was prepared in excess ligand over Fe(III) (2:3 and lower Fe/L^8 ratio), the apparent dissociation rate constants attributed to the bis complex observed in stage II_1 exhibit higher values than the dissociation rate constants observed for the complex prepared in 1:1 Fe/L^8 conditions. The observed rate increases with respect to an increase in ligand concentration, but in excess ligand over Fe(III) (Fe/$L^n \leq$ 2:4) the slope in the plot of the apparent dissociation rate constant with respect to $[H^+]$ became independent of the ligand concentration (Figure 8B). These kinetic data are interpreted according to

$$Fe(L^8H)_2^+ + H^+ \rightleftharpoons Fe(L^8H)^{2+} + H_2L^8 \quad K_7, k_7, k_{-7} \quad (26)$$

$$Fe(L^8)^+ + H^+ \rightleftharpoons Fe(L^8H)^{2+}* \quad K_5, k_5, k_{-5} \quad (27)$$

and

$$Fe(L^8H)^{2+}* \rightleftharpoons Fe(L^8H)^{2+} \quad K_6, k_6, k_{-6} \quad (28)$$

where we consider the dissociation of the species $Fe(L^8)^+$ and

$Fe(L^8H)_2^{+}$ to the mono(hydroxamato)iron(III) complex $Fe(L^8H)^{2+}$. $Fe(L^8H)^{2+}$* in reaction 28 is a bis complex with one hydroxy group protonated as is shown in Scheme 3.

The first-order absorbance decay shows that the two species, $Fe(L^8H)_2^{+}$ and $Fe(L^8)^{+}$, dissociate in the same pH range. The observed dissociation rates are dependent on the relative concentration of each species and are a function of the L^8 ligand concentration. Kinetic results suggest that at excess ligand concentrations where the dissociation rate becomes independent of the ligand concentration (Fe(III)/L^8 < 2:4), $Fe(L^8H)_2^{+}$ is the main bis-chelate species in solution. However, at conditions where Fe(III)/L^8 is 1:1, $Fe(L^8)^{+}$ is the predominant species. According to eqs 26 and 27, both reactions should exhibit first-order H^+ dependence. The dissociation rate determined in excess ligand over iron(III) is attributed to ligand dissociation from $Fe(L^8H)_2^{+}$ by assuming a small contribution from $Fe(L^8)^{+}$. The plot in Figure 8B at conditions where the Fe(III)/L^8 ratio is 2:4 was analyzed according to eq 21 to determine k_7 and k_{-7} (Table 1). The ligand dissociation rate constant determined from the plot of k_7^{obs} with respect to $[H^+]$ at 1:1 Fe(III)/L^8 ratio is attributed to the dissociation of $Fe(L^8)^{+}$. At 1:1 Fe(III)/L^8 conditions, $Fe_2(L^8)_2^{2+}$ is also present in solution; however, as we know from the L^2 ligand system, the dissociation of the $Fe_2L_2^{2+}$ species exhibits second-order H^+ dependence, and we also expect the complex to dissociate at a slower rate.

The first absorbance decay (stage II_1) is followed by two first-order absorbance *increases* (stages II_2 and II_3) and a slow absorbance decay (stage II_4) as illustrated in Figure 3B. Time-dependent spectra for stages II_2 and II_3 show an overall absorbance increase with an isosbestic point at 548 nm. The process is associated with the *formation* of a bis(hydroxamato)-iron(III) complex. The absorbance increase cannot be attributed to the complexation of free iron, since addition of excess Fe(III) or free ligand did not have any effect on the observed rate. The apparent rate constant determined by fitting the first absorbance increase as a monoexponential signal shows second-order H^+ dependence (Figure 9).

Our proposed mechanism, consistent with this behavior, takes into account the dissociation of $Fe_2(L^8)_2^{2+}$, followed by formation of $Fe(L^8)^{+}$, according to Scheme 1. The absorbance increase

Scheme 1

$$Fe_2(L^8)_2^{2+} + H^+ \rightleftharpoons Fe_2(L^8)(L^8H)^{3+} \quad K_4 \qquad (29)$$

$$Fe_2(L^8)(L^8H)^{3+} + H^+ \rightleftharpoons 2Fe(L^8H)^{2+} \quad K_3, k_3, k_{-3} \qquad (30)$$

$$Fe(L^8H)^{2+} \rightleftharpoons Fe(L^8H)^{2+}* \quad K_6^{-1}, k_{-6}, k_6 \qquad (28)$$

$$Fe(L^8H)^{2+}* \rightleftharpoons Fe(L^8)^{+} + H^+ \quad K_5^{-1}, k_{-5}, k_5 \qquad (27)$$

is attributed to the formation of the bis-chelated species $Fe(L^8)^{+}$ as a product of the $Fe_2(L^8)_2^{2+}$ dissociation. The rate of disappearance of $Fe_2(L^8)_2^{2+}$ is equivalent to the rate of formation of $Fe(L^8)^{+}$. The second-order H^+ dependence is consistent with the dissociation of $Fe_2(L^8)_2^{2+}$ as was attributed to the L^2 complex. The corresponding differential rate expression is as follows.

$$-\frac{d[Fe_2(L^8)_2^{2+}]}{dt} = \left(\frac{k_3K_4[H^+]^2}{1+K_4[H^+]} + 2k_{-3}\right)([Fe_2(L^8)_2^{2+}] - [Fe_2(L^8)_2^{2+}]_\infty) \qquad (31)$$

The apparent rate constant k_3^{obs} is expressed as shown in

$$k_3^{obs} = \frac{k_3K_4[H^+]^2}{1+K_4[H^+]} + 2k_{-3} \qquad (32)$$

The rate constant k_3 and the equilibrium constant K_4 (Table 1) are determined from a nonlinear fit of eq 32 to the experimental data (Figure 9). The intercept in Figure 9 is not precise, and no accurate result is obtained for k_{-3}.

Kinetic data for the second absorbance increase (stage II_3) were not suitable for mechanistic analysis.

The very slow absorbance decay following the two absorbance increases (stage II_4) was monitored on a 1500 s time scale at 470 nm. A monoexponential signal is observed in the $[H^+]$ range of 0.1−0.5 M. However, at higher $[H^+]$ a slight shift to biexponential behavior is observed and is probably due to ligand decomposition. This conclusion is supported by the fact that the initial absorbance intensity is not totally recovered when the pH is returned to pH = 2, where the $Fe(L^8)^{+}$ complex is stable. Kinetic traces were treated as monoexponential absorbance decays and did not account for the shift to biexponential behavior. A reasonable fit was obtained for these conditions. The slow dissociation reaction (stage II_4) is associated with ligand dissociation from a mono(hydroxamato)iron(III) complex to give free hydrated iron(III). Our kinetic data are consistent with the dual path mechanism established for dissociation of mono(hydroxamato)iron(III) complexes according to eqs 24 and 25.[28]

The apparent dissociation rate relating the dissociation of $Fe(L^8H)^{2+}$ according to a relaxation mechanism involving $Fe(H_2O)_6^{3+}$ and $Fe(OH)(H_2O)_2^{2+}$ is represented in eq 33.[28]

$$k_1^{obs} = a + b/[H^+] + c[H^+] \qquad (33)$$

$$a = k'_{-1}, \quad b = k'_1K_h(C_{tot} - [FeLH^{2+}]_e), \quad c = k_1$$

The plot in Figure 10 represents experimental data for the dissociation of $Fe(L^8H)^{2+}$ as a function of $[H^+]$. The rate constants k_1, k_{-1}, k'_1, and k'_{-1} (Table 1) were determined from a nonlinear fit of eq 33 to the experimental data.

Discussion

Overall Scheme. The multistep behavior observed during the H^+-driven ligand dissociation reactions and the total number of protons involved cannot be resolved by considering only the dissociation of a single metal complex species for either the L^2 or L^8 ligand system. Attributing the observed absorbance decays to different species dissociating in parallel pathways is necessary in order to interpret the experimental data. The species used in our overall reaction scheme are based on transient UV−visible spectra and structural investigation by ESI-MS.[19] $Fe_2(L^2)_3$, $Fe_2(L^2)_2(L^2H)_2$, and $Fe(L^2H)_3$ were taken into account for the complexes prepared with the short carbon chain dihydroxamate ligand (Figure 1, $n = 2$; L^2). $Fe_2(L^8)_3$, $Fe(L^8H)_3$, and $Fe(L^8)(L^8H)$ were considered for the complexes prepared with the long carbon chain dihydroxamate ligand (Figure 1, $n = 8$; L^8). Schemes 2 and 3 show multiple paths for the L^2/Fe_{aq}^{3+} and L^8/Fe_{aq}^{3+} systems that are consistent with the kinetic data for stage I and stage II dissociation reactions, respectively.

$Fe(L^nH)_3$ Dissociation (Scheme 2). The complexes $Fe(L^nH)_3$ (Scheme 2) adopt a monometallic trishydroxamate coordination

(28) (a)Monzyk, B.; Crumbliss, A. L. *J. Am. Chem. Soc*. **1979**, *101*, 6203. (b) Brink, C. P.; Crumbliss, A. L. *Inorg. Chem*. **1984**, *23*, 4708.

Scheme 2. Reaction Scheme for the Dissociation of the Tris(hydroxamato)iron(III) Complexes[a]

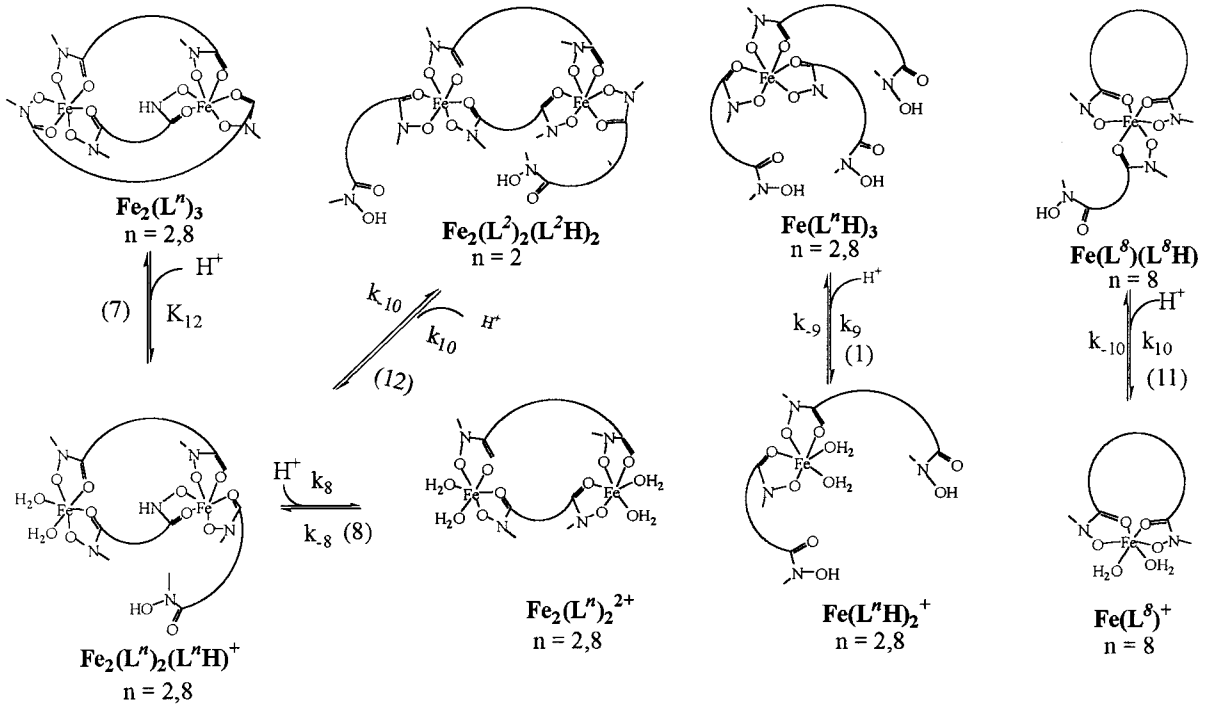

[a] Dissociated ligands and residual charges are not shown for clarity. Numbers in parentheses refer to reactions in text and in Table 1.

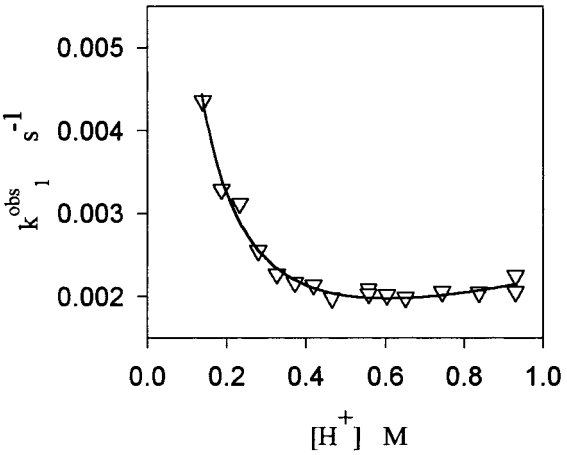

Figure 10. Stage II_3 kinetic data for the acid dissociation of (hydroxamato)iron(III) complex with ligand L^8. Observed pseudo-first-order rate constant k_1^{obsd} plotted as a function of $[H^+]$ for reactions 24 and 25. Complex is prepared in 2:3 Fe/L ratio: $[H_2L^8] = 0.2$ mM; $[Fe^{3+}] = 0.13$ mM; $I = 2.0$ M ($HClO_4/NaClO_4$); $T = 25$ °C; $[H^+] = 0.1-1.0$ M. The solid line represents an analysis of the data according to the equation $k_1^{obsd} = a + b/[H^+] + c[H^+]$ (see eq 33) where $a = 1.84 \times 10^{-4}$ (1.6×10^{-4}), $b = 5.5 \times 10^{-4}$ (2.7×10^{-5}), $c = 1.4 \times 10^{-3}$ (1.8×10^{-4}), $R^2 = 0.982$. Values in parentheses represent the standard error.

mode at neutral pH. As the pH is lowered, the complex dissociates to the bis species $Fe(L^nH)_2^+$ (eq 1). The dissociation rate constants for the L^2 and L^8 complexes are $k_9 = 3972$ and 3923 M^{-1} s^{-1}, respectively (Table 1). This similarity illustrates that the carbon chain length between the two hydroxamate units does not influence the lability of the complex in the $Fe(L^nH)_3$ binding mode. These dissociation rate constants are lower than the corresponding constants for hydroxamate ligand dissociation from $Fe(AHA)_3$ (1.0×10^5 M^{-1} s^{-1})[29] and $Fe(NMAHA)_3$ (8.6×10^3 M^{-1} s^{-1}).[30] The lower dissociation rate constant for NMAHA relative to AHA is attributed to the ability of the *N*-methyl substituent to favor delocalization of electron density onto the carbonyl function by inductive stabilization of the positive charge density on the N atom.[28] The factor of 2 lower dissociation rate constant for $Fe(L^nH)_3$ relative to $Fe(NMAHA)_3$ may be attributed to hydrophobic/solvation effects on the bimolecular reaction of solvated H_3O^+ with Fe(III) surrounded by the long hydrocarbon chains of the dihydroxamate ligands.

$Fe_2(L^n)_3$ Dissociation (Scheme 2). $Fe_2(L^8)_3$ can potentially adopt two possible structures, a bimetallic triply bridged coordination mode and a bimetallic monobridged coordination mode, as illustrated in Figure 1. In either of these two structures the two metal centers are equivalent. The bimetallic monobridged coordination mode cannot be formed with the ligand L^2, since the short carbon chain ligand cannot form the $Fe(L^2)^+$ unit because of the steric strain involved in tetracoordination to a single metal center.[21]

For the bimetallic triply bridged species the first protonation on either metal center will lead to the species $Fe_2(L^n)_2(L^nH)^+$ (Scheme 2, eq 7). This intermediate species has multiple nonequivalent protonation sites, and multiple ligand dissociation pathways are possible. We considered only the protonation sites leading to a bis complex, since tris complexes dissociate with a much higher rate than the bis complex.[1,29-31] This assumption reduces the possible products of the second protonation of $Fe_2(L^n)_3$ to $Fe_2(L^n)_2^{2+}$ and to $Fe_2(L^n)(L^nH)_2^{2+}$. The $Fe_2(L^n)_2^{2+}$ species is believed to be more stable than $Fe_2(L^n)(L^nH)_2^{2+}$, as was previously discussed for complexes of similar structure.[20] This assumption is supported by ESI-MS analysis and thermodynamic studies, where no evidence for $Fe_2(L^n)(L^nH)_2^{2+}$ was reported.[19] Consequently, we propose that ligand dissociation from $Fe_2(L^n)_3$ occurs through the intermediate species $Fe_2(L^n)_2^{2+}$. Further support of this pathway is shown in the

(29) Biruš, M.; Bradić, Z.; Kujundžić, N.; Pribanić, M.; Wilkins, P. C.; Wilkins, R. G. *Inorg. Chem.* **1985**, *24*, 3980.
(30) Caudle, M. T.; Crumbliss, A. L. *Inorg. Chem.* **1994**, *33*, 4077.
(31) Zhang, Z.; Jordan, R. B. *Inorg. Chem.* **1996**, *35*, 1571.

dissociation of the bis complex. The small difference in the dissociation rate constants for $Fe_2(L^n)_2(L^nH)^+$ in reaction 8 (k_8 = 1828 and 1495 M^{-1} s^{-1} for L^2 and L^8, respectively) is consistent with no interactions between the Fe(III) centers. The similar behavior observed for L^2 and L^8 suggests that the reaction observed for L^8 involving two H^+ is the result of triply bridged complex dissociation. This is because the monobridged complex dissociation will have as products the species $Fe(L^8)^+$ and $Fe(L^8)(L^8H)$, and the reaction would then be first-order in $[H^+]$. This conclusion, based on kinetic results that $Fe_2(L^n)_3$ is a triply bridged species, is consistent with the X-ray crystal structure of a similar complex.[18]

$Fe_2(L^2)_2(L^2H)_2$ and $Fe(L^8)(L^8H)$ Dissociation (Scheme 2). The stage I_3 dissociation process is attributed to ligand dissociation from $Fe_2(L^2)_2(L^2H)_2$ and $Fe(L^8)(L^8H)$ for the L^2 and L^8 complexes, respectively. Since the ligand L^2 cannot act as a tetradentate ligand by coordinating to a single Fe(III) center,[21] the $Fe(L^2)(L^2H)$ structure was not considered for the L^2 ligand. The reactivities of ternary complexes (Figure 2) prepared in situ support the attribution of the stage I_3 process to ligand dissociation from $Fe_2(L^2)_2(L^2H)_2$ and $Fe(L^8)(L^8H)$. By addition of the monohydroxamic acid NMAHA to the L^2 complex prepared at 1:1 Fe/L^2 conditions, we expect at neutral pH to form the complex $Fe_2(L^2)_2(NMAHA)_2$. Spectra of the ternary complex exhibit a strong absorbance band at 425 nm (ϵ = 2700−2800 M^{-1} cm^{-1} per Fe), characteristic of a trishydroxamate complex. The L^8 ternary complex prepared at the same conditions gave identical results. In addition to the equilibrium spectrophotometric data, the time-dependent spectra exhibit the same behavior observed for the dissociation of the tris-chelated L^n complex. Kinetic data are in good agreement with the assumption that for the L^2 complex we form the ternary complex $Fe_2(L^2)_2(NMAHA)_2$, since only one dissociation reaction to give a bis complex is observed. The rate constant for ligand dissociation (reaction 14) from the ternary complex $Fe_2(L^2)_2(NMAHA)_2$ is k''_{10} = 481 M^{-1} s^{-1} and agrees well with the rate constant determined for the stage I_3 path for the L^2 complex $Fe_2(L^2)_2(L^2H)_2$ in reaction 12 (k_{10} = 422 M^{-1} s^{-1}; Table 1). The same agreement is obtained between $Fe(L^8)(L^8H)$ and the ternary complex of L^8 and NMAHA, $Fe(L^8)(NMAHA)$. Proton-driven ligand dissociation from $Fe(L^8)(NMAHA)$ (reaction 13) is observed with k'_{10} = 316 M^{-1} s^{-1}, which agrees with ligand dissociation kinetics from $Fe(L^8)(L^8H)$(stage I_3; reaction 11, k_{10} = 284 M^{-1} s^{-1}). The $Fe_2(L^2)_2(NMAHA)_2$ complex dissociates in two steps to give the bis complex $Fe_2(L^2)_2^{2+}$. The fact that we observe only one reaction shows that the two metal centers are not interacting and that the presence of one positive charge on one side of the complex does not affect the protonation reaction at the second neutral metal center. This result is in good agreement with a noninteraction assumption between the two metal centers.[27]

It is interesting to compare ligand dissociation rates for tris-chelated Fe(III) in the ternary complexes with the dissociation of the tris complexes $Fe(AHA)_3$ and $Fe(NMAHA)_3$ (Figure 2). The following reactions will serve to illustrate this comparison. In all of the reactions the dissociation consists of the removal of a single hydroxamic acid unit from the first coordination shell of the tris-chelated metal center (coordinated water not shown for clarity).

$$Fe(AHA)_3 + H^+ \rightarrow Fe(AHA)_2^+ + HAHA \quad (34)$$

$$k = 1.0 \times 10^5\ M^{-1}\ s^{-1} \quad \text{(ref 29)}$$

$$Fe(NMAHA)_3 + H^+ \rightarrow Fe(NMAHA)_2^+ + HNMAHA \quad (35)$$

$$k = 8.0 \times 10^3\ M^{-1}\ s^{-1} \quad \text{(ref 30)}$$

$$Fe(L^8H)_3 + H^+ \rightarrow Fe(L^8H)_2^+ + H_2L^8 \quad (36)$$

$$k = 4.0 \times 10^3\ M^{-1}\ s^{-1}$$

$$Fe(L^8)(AHA) + H^+ \rightarrow Fe(L^8)^+ + HAHA \quad (37)$$

$$k = 4.5 \times 10^3\ M^{-1}\ s^{-1}$$

$$Fe(L^8)(NMAHA) + H^+ \rightarrow Fe(L^8)^+ + HNMAHA \quad (38)$$

$$k = 3.2 \times 10^2\ M^{-1}\ s^{-1}$$

$$Fe(L^2H)_3 + H^+ \rightarrow Fe(L^2H)_2^+ + H_2L^2 \quad (39)$$

$$k = 4.0 \times 10^3\ M^{-1}\ s^{-1}$$

$$Fe_2(L^2)_2(NMAHA)_2 + 2H^+ \rightarrow Fe_2(L^2)_2^{2+} + 2HNMAHA \quad (40)$$

$$k = 4.8 \times 10^2\ M^{-1}\ s^{-1}$$

One feature appears evident once an allowance is made for the difference in ligand dissociation rates between N−H and N−CH_3 hydroxamic acids. The ternary complexes appear to be less reactive with respect to hydroxamic acid ligand dissociation, even when statistical factors are taken into account (one vs three potential dissociating ligands). The hydrophobicity of the hydrocarbon connecting chain in the dihydroxamate complexes appears to diminish H^+-activated ligand dissociation. The effect is most pronounced when the dihydroxamate is acting as a tetradentate ligand, that is, when the hydrocarbon connecting chain is confined in proximity to the inner coordination shell of the Fe(III) reactive site. This is illustrated by the 20-fold decrease in rate constant for AHA dissociation from $Fe(L^8)(AHA)$ (reaction 37) relative to $Fe(AHA)_3$ (reaction 34) and by the 30-fold decrease in rate constant for NMAHA dissociation from $Fe(L^8)(NMAHA)$ (reaction 38) relative to $Fe(NMAHA)_3$ (reaction 35). The increased hydrophobic effectiveness when the dihydroxamate hydrocarbon chain is held in proximity to the Fe(III) inner coordination shell is further illustrated by the minimal factor of 2 difference in comparing dissociation rates for $Fe(NMAHA)_3$ (reaction 35) with those for $Fe(L^8H)_3$ and $Fe(L^2H)_3$ (reactions 36 and 39). The hydrophobic effect is also seen in the dinuclear ternary complex in that NMAHA dissociation from $Fe_2(L^2)_2(NMAHA)_2$ (reaction 40) is 20-fold less than from $Fe(NMAHA)_3$ (reaction 35). Apparently the presence of an adjacent Fe(III) center does not influence ternary complex reactivity.

Ligand Dissociation from Different Bishydroxamate Complex Structures (Scheme 3). The dissociation of the various tris-chelated complexes in stage I provides multiple paths to the bis-chelated structures $Fe_2(L^n)_2^{2+}$ (n = 2, 8), $Fe(L^nH)_2^+$ (n = 2, 8), and $Fe(L^n)^+$ (n = 8) (Scheme 2). The multistep behavior observed for the bis complex dissociation illustrated in Scheme 3 for stage II is in good agreement with the proposed mechanism for tris(hydroxamato)iron(III) complex dissociation.

The bis(hydroxamato)iron(III) complex for the short carbon chain ligand L^2 was investigated in a 1:1 Fe/L^2 ratio by ESI-MS and found to adopt a bimetallic doubly bridged binding mode $Fe_2(L^2)_2^{2+}$.[21] Our previous kinetic investigation at the same conditions supports the electrospray structural analysis.[20,21]

Scheme 3. Reaction Scheme for the Dissociation of the Bis(hydroxamato)iron(III) Complexes[a]

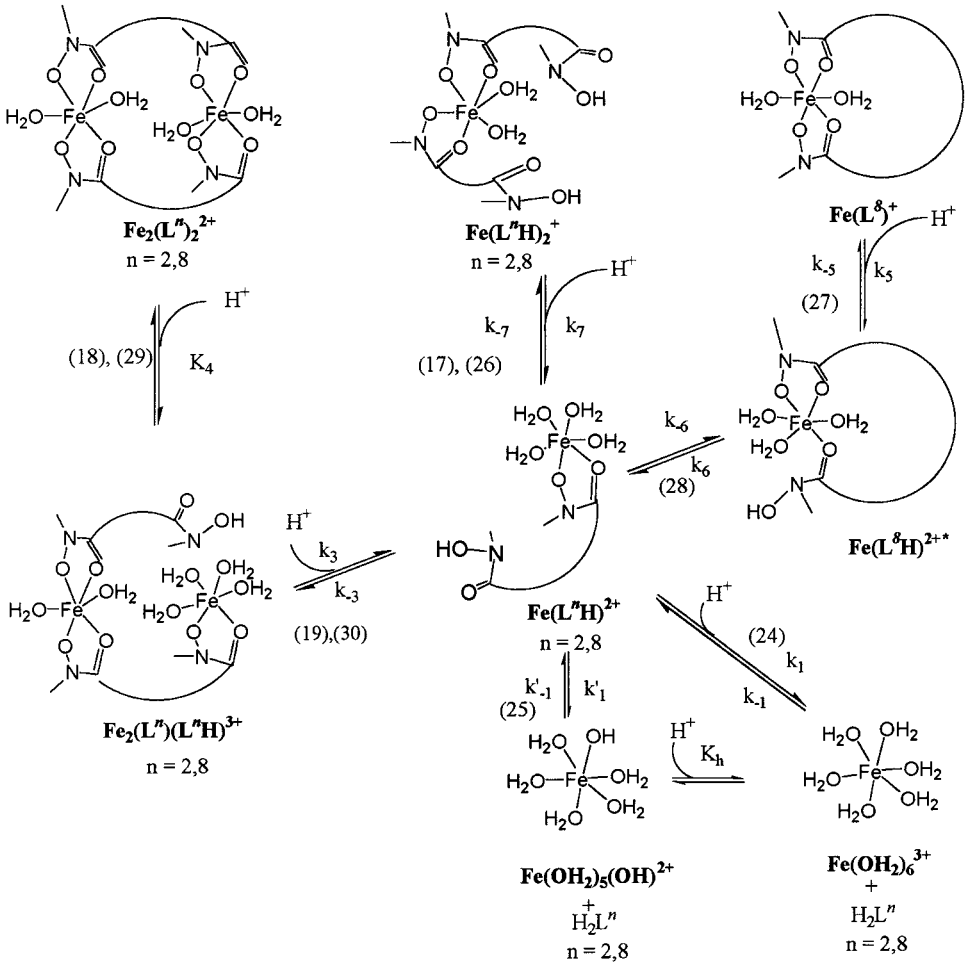

[a] Dissociated ligands and residual charges are not shown for clarity. Numbers in parentheses refer to reactions in text and in Table 1.

However, in the present work the bis complex of L^2 formed as a transient in the dissociation of higher complexes prepared at a 2:3 Fe/L^2 ratio shows two distinct and well-separated dissociation steps in stage II. The spectral changes in both cases are consistent with bis complex dissociation (Supporting Information, parts A and B of Figure S2). The first step, stage II_1, is attributed to the dissociation of the mono-Fe complex $Fe(L^2H)_2^+$ (Scheme 3, eq 17). The rate constant for H^+-dependent ligand dissociation of this species, $k_7 = 92\ M^{-1}\ s^{-1}$, is in the expected range for the dissociation of an *N*-methyl hydroxamate ligand from a bishydroxamate complex. For example, the rate constant for H^+-driven dissociation of NMAHA from $Fe(NMAHA)_2^+$ is $k = 100\ M^{-1}\ s^{-1}$.[30] This assignment also supports the designation of the first ligand dissociation step in the tris complex to the $Fe(L^2H)_3$ species, since at a 1:1 Fe/L^2 ratio the main species in solution is $Fe_2(L^2)_2^{2+}$, as was demonstrated previously.[20] We also conclude that $Fe(L^2H)_2^+$ is not present when the complex is formed at 1:1 Fe/L^2 conditions, since kinetic data at these conditions do not support its presence.

The same result was obtained for the L^8 complex. The H^+-driven ligand dissociation rate constant for $Fe(L^8H)_2^+$ is $k_7 = 65\ M^{-1}\ s^{-1}$ (Scheme 3, eq 26), in reasonable agreement with the corresponding value for ligand dissociation from $Fe(L^2H)_2^+$ and $Fe(NMAHA)_2^+$ (see above). It is probable that for the L^8 ligand with a long carbon connecting chain, even in a large excess of ligand over Fe, the species $Fe(L^8)^+$ is still present in an appreciable amount. The rate constant for the dissociation of $Fe(L^8)^+$ determined from 1:1 Fe/L^8 conditions should not be affected by the presence of $Fe(L^8H)_2^+$, since this species is produced by the dissociation of $Fe(L^8H)_3$ and is not detected at 1:1 Fe/L^8 conditions. However, at 1:1 Fe/L^8 conditions, $Fe_2(L^8)_2^{2+}$ is also present in solution and the observed dissociation rates for $Fe(L^8)^+$ can be affected by ligand dissociation from $Fe_2(L^8)_2^{2+}$. In our previous study the L^8 complex prepared at 1:1 Fe/L^8 conditions was considered as a mono-Fe complex $Fe(L^8)^+$ on the basis of an ESI-MS investigation. We recently demonstrated by an ESI-MS investigation of Ga(III)−Fe(III) mixed complexes that the complex prepared at 1:1 Fe/L^8 conditions can adopt both mono- ($Fe(L^8)^+$) and bimetallic ($Fe_2(L^8)_2^{2+}$) structures.[19]

In this study the dissociation of $Fe_2(L^8)_2^{2+}$ is observed with an increase in the absorbance, which is attributed to the rapid transformation of the intermediate $Fe(L^8H)^+$ to the more stable $Fe(L^8)^+$ complex (Scheme 3, eqs 28 and 27). This behavior is not observed for $Fe_2(L^2)_2^{2+}$ dissociation, since the ligand L^2 cannot bind both hydroxamate units to a single Fe(III) center because of steric strain (i.e., cannot form $Fe(L^2)^+$), and therefore, the intermediate species $Fe(L^2H)^+$ undergoes ligand dissociation to $Fe(H_2O)_6^{3+}$ and $Fe(OH)(H_2O)_5^{2+}$ (Scheme 3).

An absorbance increase during the course of ligand dissociation was reported for ferrioxamine B dissociation and was attributed to complexation of Fe_{aq}^{3+} present in solution.[32] In

our study the absorbance increase in stage II for the L^8 complex cannot be attributed to the complexation of Fe_{aq}^{3+}, since addition of excess Fe(III) in the acidic solution did not have any effect on the observed rate, nor did the presence of free ligand. The second-order H^+ dependence is consistent with the dissociation of $Fe_2(L^8)_2^{2+}$ as was observed for the corresponding L^2 complex. The rapid dissociation of $Fe_2(L^8)_2^{2+}$ led to a rapid increase in the concentration of $Fe(L^8H)^{2+}$ that underwent a slow ligand dissociation reaction via parallel paths producing $Fe(H_2O)_6^{3+}$ and $Fe(OH)(H_2O)_5^{2+}$. In addition, $Fe(L^8H)^{2+}$ is in equilibrium with $Fe(L^8)^+$ according to eqs 28 and 27. The fast increase in $Fe(L^8H)^{2+}$ concentration displaces equilibria 28 and 27 in the direction of formation of $Fe(L^8)^+$. Reaction 28 is a rapid ring-closure process that we expect to be controlled by the dissociatively activated rate of water exchange from the inner coordination sphere of $Fe(L^8H)(OH_2)_4^{2+}$. Therefore, it is not surprising that we observe that $Fe(L^8)^+$ formation kinetics are controlled by the rate of the dissociation of $Fe_2(L^8)_2^{2+}$; i.e., $Fe(L^8)^+$ is formed at the rate of $Fe_2(L^8)_2^{2+}$ dissociation.

The second absorbance increase in stage II is probably also due to the formation of the $Fe(L^8)^+$ complex as a result of the transformation of $Fe(L^8H)^{2+}$ produced by the dissociation of Fe $(L^8H)_2^+$. The observed rate is slower than in the previous step (stage II_2) probably because of the steric requirements associated with ligand rotation to be in a suitable position for Fe(III) chelation; therefore, the formation kinetics are limited by the rate of ligand conformational change rather than displacement of H_2O from the first coordination shell of the ligand-substituted Fe(III). Kinetic results for this step were not suitable for analysis, and our data do not show strong arguments to confirm this assignment.

Dissociation of the Mono(hydroxamato) Complex (Scheme 3). Dissociation of the mono(hydroxamato)iron(III) species $Fe(L^nH)^{2+}$ proceeds by a parallel path mechanism to produce $Fe(H_2O)_6^{3+}$ and $Fe(H_2O)_5OH^{2+}$ (Schemes 2 and 3) as previously reported.[20,28,30] Further discussion of this final step may be found in these references.

Electrostatic Effects in Di-Fe Species. The mechanism of ligand dissociation from the bimetallic complex $Fe_2(L^n)_2^{2+}$ is of particular interest for studying electrostatic effects on the dissociation rate. In the bimetallic doubly bridged complex $Fe_2(L^n)_2^{2+}$ the two metal centers are equivalent with a residual +1 charge on each metal. Protonation at either metal site gives $Fe_2(L^n)(L^nH)^{3+}$ (reaction 18 or reaction 29; Scheme 3) in which the two Fe(III) centers have 1+ and 2+ residual charges. If the assumption of noninteraction between the two metal centers is valid, then any additional activation barrier observed in ligand dissociation from the bishydroxamate site in $Fe_2(L^n)(L^nH)^{3+}$ over that in $Fe_2(L^n)_2^{2+}$ should be accounted for by electrostatic repulsion of the incoming H^+ from the adjacent Fe(III) center carrying a residual 2+ charge. A model for pure Coulombic repulsion was proposed[20] and discussed considering the energy difference between the (1+, 2+) and (2+, 2+) charge-separated species, which represents the energy needed to bring one H^+ to the Fe(III) center of 1+ residual charge by countering the repulsion of the 2+ charge on the second Fe(III) center. This is illustrated by

$$\Delta E = \frac{(+2)(+2)e^2}{\epsilon r} - \frac{(+2)(+1)e^2}{\epsilon r} = \frac{2e^2}{\epsilon r} \qquad (41)$$

where r represents the distance separating the two charges and

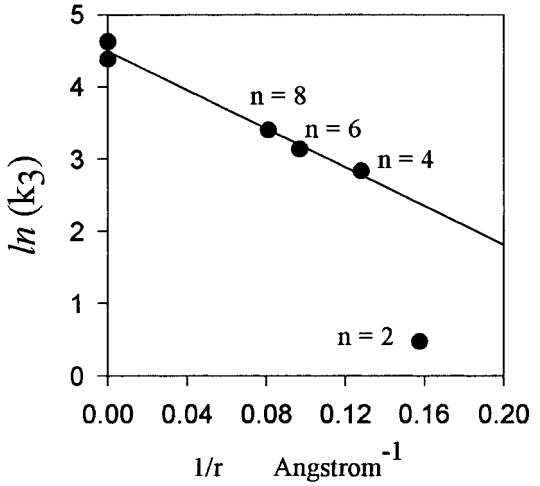

Figure 11. Influence of Fe−Fe distance on the rate constant for H^+-driven ligand dissociation from $Fe_2(L^n)(L^nH)^{3+}$. Logarithm of the rate constant for reactions 19 and 30 is plotted as a function of the reciprocal of the Fe−Fe distance, estimated from molecular mechanics conformational studies.[21] The n values represent the length of the C atom chain between hydroxamate groups. Data for $n = 4$ and $n = 6$ are from ref 20, k_3 values at $1/r = 0$ are for $Fe(NMAHA)_2$[30] and $Fe(L^2H)_2^+$. A linear fit of eq 43 to all the data gave a slope and intercept of −20.65 and 4.7, respectively ($R^2 = 0.83$) and a calculated value of $\epsilon = 53$. Omitting the $n = 2$ data point from statistical analysis according to eq 43 gave a slope and intercept of −13.4 and 4.49, respectively (line shown $R^2 = 0.98$), and a calculated value of $\epsilon = 82$. See text.

ϵ represents the dielectric constant of the medium. If we assume that the intrinsic activation barrier in the protonation of the bis(hydroxamato)iron(III) ligand dissociation is constant (i.e., independent of the distance between the two Fe centers), then the energy barrier $\Delta G^{\#}$ for H^+-driven ligand dissociation from the $Fe_2(L^n)(L^nH)^{3+}$ complex in reactions 19 or 30 (Scheme 3) is composed of an intrinsic barrier and an electrostatic barrier. Equation 42 was derived on this basis. On the basis of this relationship, the activation barrier for the dissociation rate constant k_3 can be expressed as

$$\Delta G^{\ddagger} = \frac{2e^2NC}{\epsilon r \times 10^{-8}} + \Delta G^{\ddagger}_{\text{int}} \qquad (42)$$

where e is the electrostatic charge (4.80×10^{-10} esu), N is Avogadro's number (6.023×10^{23}), C is 1×10^{-7} J/erg, and r is the Fe−Fe distance in angstroms. This may be expressed in terms of the microscopic rate constant (k_3) for reactions 19 and 30 (Scheme 3) as shown

$$\ln k_3 = (-1.1 \times 10^3)\left(\frac{1}{\epsilon r}\right) + \ln k_{3(\text{int})} \qquad (43)$$

According to eq 43, $\ln k_3$ should vary linearly with respect to $1/r$ with a slope inversely related to the dielectric constant of the medium. A plot of $\ln k_3$ vs $1/r$ is illustrated in Figure 11. The rate constant (k_3) for ligand dissociation from $Fe_2(L^n)(L^nH)^{3+}$ decreases with decreasing distance between the two Fe(III) centers, in agreement with the proposed model. In Figure 11, the rate constant for ligand dissociation from $Fe(NMAHA)_2^+$ or $Fe(L^nH)_2^+$ is considered as a measure of the intrinsic reactivity, $k_{3(\text{int})}$; that is, the monometallic complex represents the case where the second charged Fe(III) center is an infinite distance away from the reaction center, and therefore, no neighboring group electrostatic effects are operative. When all

(32) Biruš, M.; Bradić, Z.; Krzanric, G.; Kujundžić, N.; Pribanić, M.; Wilkins, P. C.; Wilkins, R. G. *Inorg. Chem.* **1987**, *26*, 1000.

of the data are considered in Figure 11, the slope of the plot yields an estimated dielectric constant ϵ for the medium separating the two Fe(III) centers in $Fe_2(L^n)(L^nH)^{3+}$ as 53. However, the data point for $n = 2$ deviates significantly from this line, and the correlation of the data excluding the $n = 2$ ligand (line shown) gives a dielectric constant of 82. The dielectric constant of water in 2.0 M $NaClO_4$ (our reaction conditions) is reported to be 53.44,[33] and the dielectric constant of pure water is 78. This result suggests that the solvent composition in proximity to the Fe(III) centers in $Fe_2(L^n)(L^nH)^{3+}$ is different from the bulk medium. The fact that the data point for the very short chain length ligand ($n = 2$) deviates from the linear correlation is probably due to a breakdown in the continuum assumption, since the cavity between the two metal centers does not contain solvent molecules. A crystal structure for $Fe_2(L^2)_2^{2+}$ shows that no solvent molecules are held between the two Fe(III) centers.[34]

(33) Barthel, J.; Buchner, R.; Munsterer, M. In *Electrolyte Data Collection. Part 2: Dielectric Properties of Water and Aqueous Electrolyte Solutions*; Chemistry Data Series; DECHEMA: Frankfurt, Germany, 1995; Vol. XII, Part 2, p 206.

(34) Boukhalfa, H.; Crumbliss, A. L. Manuscript in preparation.

Conclusion

Proton-driven ligand dissociation from tris-chelated dihydroxamato complexes of Fe(III) proceeds through multiple parallel paths to Fe_{aq}^{3+} products. It is the multiple species and multiple reaction paths that distinguish the ligand exchange chemistry of the tetradentate dihydroxamate siderophores from their hexadentate and bidentate counterparts. These multiple pathways, and the additional lability that they afford the dissociating Fe(III), may play a role in dihydroxamate siderophore mediation of Fe bioavailability and may be a rationale for their biosynthesis, despite the higher environmental ligand concentrations required for complete Fe(III) chelation relative to their hexadentate counterparts.

Acknowledgment. We gratefully acknowledge financial support from the NSF and the Burroughs-Wellcome Fund.

Supporting Information Available: Three Figures containing time-dependent UV−visible spectra of the tris(hydroxamato)iron(III) complex and bis(hydroxamato)iron(III) complex dissociation for L^2 and L^8 complexes. This material is available free of charge via the Internet at http://pubs.acs.org.

IC0001659